NRL Report 7423

The NRL OSO-4 Bragg Crystal Spectrometer Instrument

J. F. MEEKINS

Upper Air Physics Branch
Space Science Division

July 27, 1972

NAVAL RESEARCH LABORATORY
Washington, D.C.

CONTENTS

ABSTRACT

Two Bragg crystal spectrometers were placed on the OSO-4 satellite to study solar flare plasmas by their spectral emissions. The solar flare plasma parameters were measured with these spectrometers, which together covered a total wavelength range of 0.6 to 8.4 Å. With these instruments, knowledge could be gained into the mechanisms governing the plasma behavior in the high temperature-low density regime of flare production and in solar evolution and elemental abundances in the sun. However, spacecraft limitations forced many restrictions on the design of the instrument, so the final instrument could not measure all the solar flare plasma state parameters.

PROBLEM STATUS

This is an interim report; work is continuing.

AUTHORIZATION

NRL Problem A01-29
Project S-99805-G

Manuscript submitted April 11, 1972.

THE NRL OSO-4 BRAGG CRYSTAL SPECTROMETER INSTRUMENT

INTRODUCTION

The NRL Bragg crystal spectrometers were placed in the pointed section of the OSO-4 satellite to study solar flare plasmas by their spectral emissions. These spectra are one of the few tools available for the study of the hot, tenuous plasmas characteristic of solar flares. Since solar flare plasmas were expected to have temperatures in excess of 10^7 K, the most sensitive spectra (in terms of plasma parameters) would be in the wavelength region below 10 Å. Theoretically, this spectral region includes line emission from the nearly stripped ions of the elements Mg, Al, Si, S, Ar, Ca, and Fe. Continuum emission should also result from free-free (bremsstrahlung) and free-bound (recombination) electron transitions.

It was considered possible that the continuum would result from collisions of energetic electrons with a relatively less energetic plasma. In such a case, initially at least, the x-ray spectrum in the region less than 10 Å would show a continuum representative of the electron velocity distribution but a line emission characteristic of the cooler plasma, e.g., line emission from inner shell electron transitions. On the other hand, if the electron energy distribution was nearly the same as that of the ions with which these electrons interacted, the emission would be consistent with that expected from a plasma in thermal equilibrium. Since Doppler line profiles reflect the ion temperature, for thin plasmas in relatively weak magnetic fields, line width would be a further diagnostic of the plasma state.

The experiment objective then was to determine the parameters which would describe the solar flare plasma state. To obtain this objective, two Bragg crystal spectrometers were used, which in combination covered the total wavelength range of 0.6 to 8.4 Å. To meet the low power requirements on the OSO-4 spacecraft and provide a reliable instrument (one operating longer than 1 year in orbit), a stepping motor was selected to drive the spectrometer. (A constant-speed dc motor requires more power than was available.) Previous measurements had also indicated that the solar flare emission may undergo changes of greater than an order of magnitude in this wavelength range in just a few minutes of time. Spacecraft limitations forced many restrictions on the design of the instrument, so the final instrument could not measure all the parameters required to describe the solar flare plasma state. These restrictions included:

1. The selection of crystals with limited area required relatively long integration times to obtain a sufficient number of counts from lines and continuum radiation of the solar spectrum below 10 Å. Thus, the scan rate over the spectral range had to be rather slow.

2. The wavelength resolution had to be reduced (one spectrometer step = 0.1 degree) to acquire some information on the time history of the x-ray emission in various parts of the spectrum during a flare. Accurate measurements of line intensities required

the crystals' rocking curves to be greater than or equal to the width of one spectrometer step. Satisfying this requirement assured that no line would be stepped over.

3. Fine collimation and offset pointing to flare regions were not possible, so accurate measurements of line profiles could not be made from OSO-4.

Figure 1 shows the main components of the NRL instrument, and Fig. 2 indicates the location of the instrument in the OSO-4 spacecraft.

DETAILS OF THE INSTRUMENT

X rays are diffracted from crystals according to Bragg's Law:

$$n\lambda = 2d \sin\theta ,$$

where n is any positive integer (representing order of diffraction), λ is the wavelength, d is the spacing between atomic planes in the crystal, and θ is the angle between the atomic planes of the crystal and incident x-ray beam as well as between the atomic planes and the diffracted beam. The maximum wavelength that can be diffracted is 2d. X-ray wavelengths may be measured with the Bragg crystal spectrometer diagrammed in Fig. 3. Typically, the diffracting crystal is at the center of the spectrometer with a detector viewing the diffracted emission. To satisfy the Bragg relation for all angles θ the spectrometer requires a simple coupling between the crystal and the detector such that the detector rotates at twice the angular rate of the crystal.

The requirements of the NRL experiment indicated that the spectral range between 1 and 8 Å could best be covered by a two-range spectrometer. The two-range system is composed of two sealed halogen-quenched Geiger counters with mica windows, a lithium flouride crystal ($2d \approx 4$ Å), and an ethylene diamine d-tartrate (EDDT) crystal ($2d \approx 8.8$ Å).

The Geiger counters, which were 1.87 cm deep, were filled to a pressure of 650 mm Hg with 1% bromine in argon. The filling pressure was determined by requiring a reasonable quantum efficiency ($\approx 1\%$) at 1 Å while keeping the tube operating voltage reasonably low (≈ 1200 V). The halogen quench (bromine) was chosen to prevent permanent degradation of the tube operating characteristics due to large numbers of accumulated counts expected from the South Atlantic Anomaly. Mica (≈ 1.5 mg/cm^2) was selected for the window material because of its compatibility with the halogen quench. Individual detectors were selected for flight by requiring that they have a threshold (the minimum voltage at which the tube is operating in the Geiger region) of 1150 ± 10 volts, a plateau length (range in voltage over which the tube operates in the Geiger region) of 400 volts or greater, and a plateau slope of less than 4%/100 volts. In orbit, gas can only leak out, lowering the threshold voltage, so the operating voltage was chosen to be 1200 volts near the lower end of the plateau. By culling the counters in this way, the life expectancy in orbit was greater than 1 year. At this voltage and with the electronics used, the dead time was 200 μsec (Appendix A).

Due to the size of the spectrometer step (0.1 degree), there was the possibility that the peak of a spectral line would be missed, i.e., stepped over. Two reasonable design alternatives were possible to insure observation of the peak of a spectral line: either choose crystals for flight which have wide rocking curves ($\gtrsim 0.1$ degree) or bend the crystals to

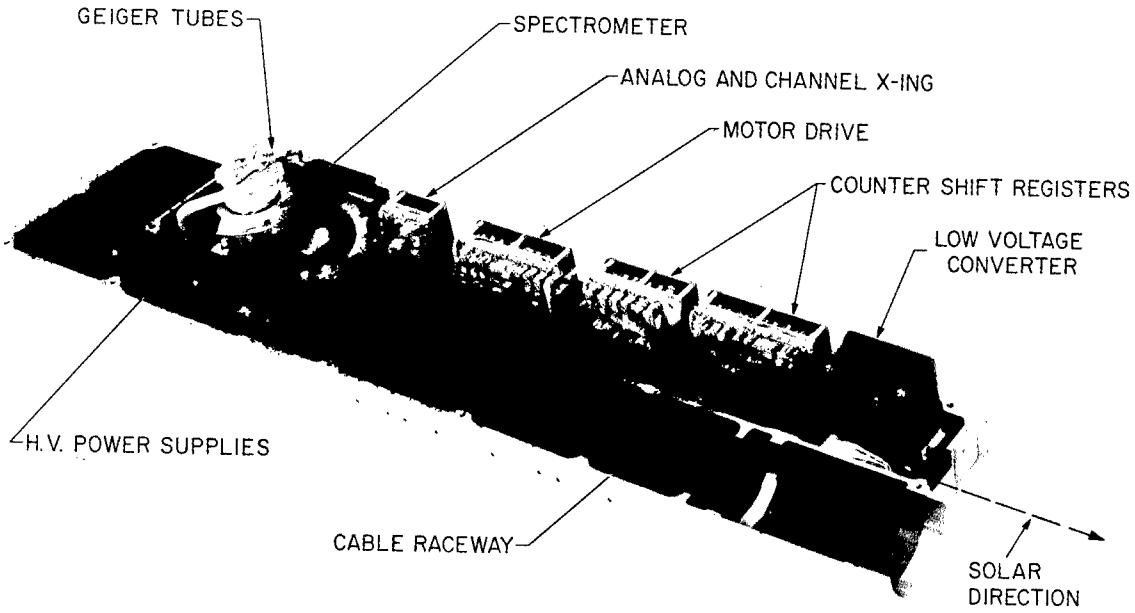

Fig. 1—The NRL OSO-4 instrument indicating the main components

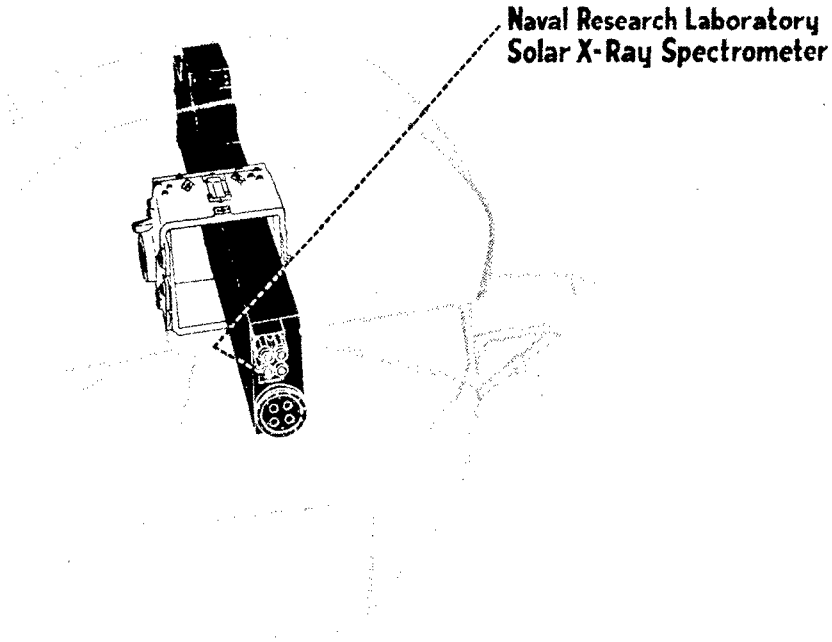

Fig. 2—Schematic showing the NRL instrument (mated to the AS&E package) mounted in the OSO-4 spacecraft

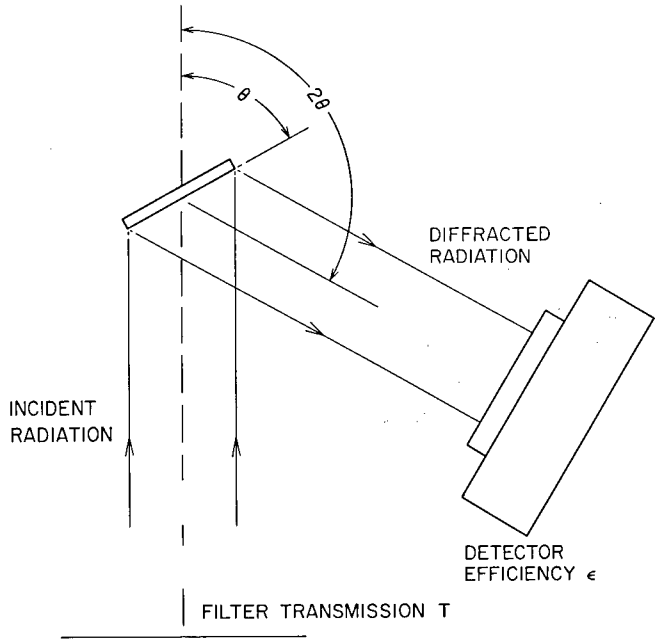

Fig. 3—Bragg crystal spectrometer showing the principal components and x-ray path

0.1 degree (Appendix B). Bending the crystals, if possible, was preferred since this technique effectively produces a crystal with a square-wave rocking-curve width of 0.1 degree, whereas a crystal with a broad rocking curve $\gtrsim 0.1$ degree diffracts appreciable radiation in the wings of the curve (i.e., at angles greater than 0.05 degree from the center). Two response curves are compared in Fig. 4. Available techniques at the time of construction indicated that only the EDDT could be bent so that the rocking curve deviated less than 10% from calculations for a uniform bend. Since this small bend is within the elastic limits of the crystal, the EDDT crystal was bent by mounting it on an aluminum substrate and bending the substrate (Fig. 5). In the final flight configuration, the EDDT crystal was bent on a right circular cylinder so that the subtended angle equals the angle of a spectrometer step (0.1 degree), and the LiF crystal was chosen for its broad rocking curve width (≈ 0.3 degree FWHM).

EDDT is by far the more sensitive to handling of the two types. After an 8-hour exposure to a relative humidity of approximately 50%, the reflectivity of EDDT was permanently decreased by over 10%. Elaborate precautions were taken throughout the test and flight programs to insure an environment with less than 30% relative humidity.

The detectors are mounted on a common arm which is rotated through 132 degrees. The detectors and crystals are geared such that the detectors receive diffracted radiation (at 2θ) from its associated crystal, and the source (solar flare) serves as the entrance slit to the spectrometers. A filter consisting of an approximately 2000 Å-thick aluminum layer evaporated on 1/4-mil Mylar film was placed over the entrance aperture to reduce solar heating of the interior of the package and to reduce low-energy particle contamination.

The telemetry data system employed by the OSO-4 spacecraft consisted of 32 eight-bit words. Since each eight-bit word is 20 msec long, it takes 640 msec to sample (or transmit) the entire 32 words. This group of 32 words is called the main frame (MF)

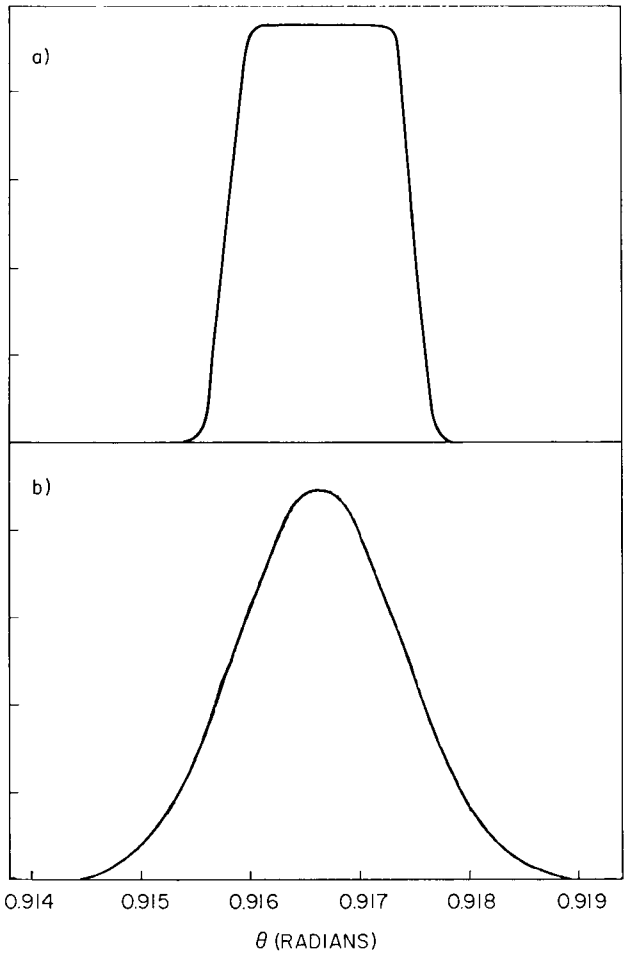

Fig. 4—Comparison of the response curves (a) A bent crystal having a narrow rocking curve (b) A flat crystal having a rocking curve

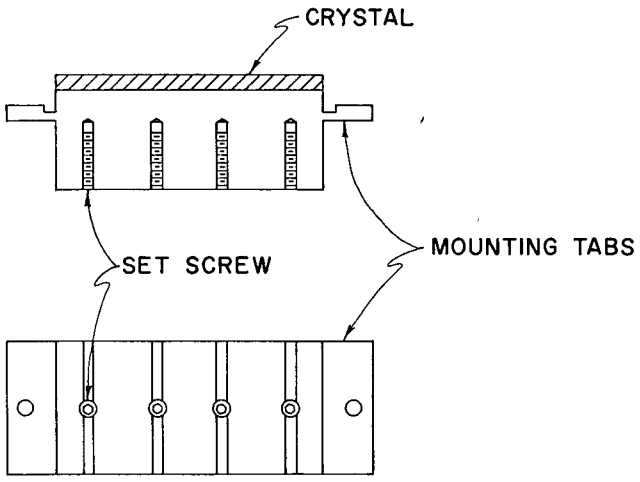

Fig. 5—The aluminum substrate used for bending the EDDT crystals

data channel. The fifteenth word was subcommutated into 48 words called the analog subcommutator 2 (ASC-sail) for the pointed-section instruments and housekeeping. The sixteenth word was subcommutated into 48 words called the analog subcommutator 1 (ASC-wheel) for the wheel instruments and housekeeping. The twenty-ninth word of the MF was subcommutated into 40 words called the digital submultiplexer (DSM). The NRL pointed instrument used main frame words 2, 13, and 23 (MF2, MF13, and MF23), DSM words 21 and 22 (DSM21 and DSM22), and ASC-sail words 35 and 36 (ASC35 and ASC36). Table 1 identifies the use of these words.

The counters and crystals are rotated by a stepping motor and precision gear train, and the position of the spectrometer (θ) is read out using a counter-shift register which counts the pulses driving the stepping motor, accumulated from the time the direction of the spectrometer is reversed. The output from each of the two Geiger counters during a sampling period is fed into other counter-shift registers, accumulated from the time of the last data readout of the counter-shift register. Table 1 gives data on accumulation times and spectrometer data word assignments for the various modes.

A block diagram of the electronic system is presented in Fig. 6. The electronics are powered by the spacecraft during satellite day; power is not needed during satellite night. In Fig. 6, tube A is the Geiger tube for the EDDT crystal; tube B is the Geiger tube for the LiF crystal. The angle of the spectrometer arm is advanced in increments of 0.2 degree (0.1 degree of crystal rotation) by the stepping motor. One pulse from a motor driver on any one of the motor coils will rotate the motor rotor 90 degrees and the spectrometer arm 0.2 degree. The sequence in which the coils are pulsed determines the direction of rotation, and the sequence reverses direction when either of the stop limit switches (at $2\theta \approx 18$ degrees and $2\theta \approx 144$ degrees) are actuated by the arm.

The stepping pulses are generated by one of the two motor drivers and sequenced to the four stepping motor coils. The pulses are triggered by the leading edges of the main frame data readout gates 2, 13, and 23. At the slow-stepping rate, a pulse is generated every other main frame by gate 2 (66 degrees of scan in approximately 13 minutes); at the fast rate, a pulse is generated by every gate, every frame (66 degrees of scan in approximately 2 minutes) (Fig. 7). This also builds in a scale factor of 2 for the data accumulated in counter-shift register B (normally the output from tube A for EDDT).

The fast pulse frequency is about 281 pulses per minute and the slow frequency is about 47 pulses per minute. The stepping pulses are generated continuously until the spectrometer arm contacts either the 18-degree or 144-degree stop. The stop generates an electrical signal which changes the pulse sequence such that the spectrometer is driven away from the stop.

Only one motor driver is in operation at any one time and either can be selected by spacecraft commands. Command 9 (spacecraft command 131 or S/C 131) latches the motor driver select relay to supply power to motor driver 1, while command 10 (S/C 132) latches the relay to supply motor driver 2.

The fast and slow speeds can be selected by both the motor driver select commands (9 and 10) and another pair of commands, 7 (S/C 129) and 8 (S/C 130). When command 9 (driver 1) has been sent, command 7 selects the fast speed and command 8 selects the slow speed. When command 10 (driver 2) has been sent, command 7 selects the slow speed and 8 the fast speed. Thus, either of two commands can be used to change speed.

Table 1
Telemetry Word Usage

Data Word	Word Bits	Parameter
MF2	ABCDEFGH	Accumulated counts since last MF readout (640 ms) { DSM-J = 1: LiF, tube B DSM-J = 0: EDDT, tube A } Count = (BCDEFGH) × 2^{3A}
MF13, MF23	ABCDEFGH	Accumulated counts since last MF23 or MF13 readout (200 ms or 440 ms resp.) { DSM-J = 0: LiF, tube B DSM-J = 1: EDDT, tube A } Count = (BCDEFGH) × 2^{3A}
DSM21 DSM22	ABCDEFGH IJKLMNPQ	Spectrometer position in motor steps since last stop and housekeeping Steps = PQABCDEFGH { I = 1: Low voltage 1 on I = 0: Low voltage 2 on J = 1: MF2 from LiF, tube B J = 0: MF2 from EDDT, tube A { KL = 11: Mtr Div 1 fast KL = 10: Mtr Div 1 slow KL = 01: Mtr Div 2 slow KL = 00: Mtr Div 2 fast { M = 0: Spectrometer is moving from 18° stop to 144° stop M = 1: Spectrometer is moving from 144° stop to 18° stop { N = 1: Spectrometer position is in error due to coming out of darkness N = 0: Position is correct
ASC35	ABCDEFGH	1. HV 1 monitor 1100 to 1300 volts ABCDEFGH = 117 to 93 (resp.) ABCDEFGH = 255: HV 1 off 2. HV 2 monitor 1100 to 1300 volts ABCDEFGH = 95 to 75 (resp.) ABCDEFGH = 255: HV 2 off 3. +4-volt monitor ABCDEFGH = 123 to 151 4. Package temperature -10 to 40° C ABCDEFGH = 123 to 101 (resp.) 1, 2, 3, 4 are commutated within the NRL package

Table 1
Telemetry Word Usage—Continued

Data Word	Word Bits	Parameter
ASC36	ABCDEFGH	Crystal temperature +20° to 50° C ABCDEFGH = 242 to 198 (resp.)
ASC 3, 9, 12, 24	ABCDEFGH	Raster position azimuth ≈±20 arc min
ASC 6, 14, 18, 42, 47	ABCDEFGH	Raster position elevation ≈±20 arc min
ASC 29	ABCDEFGH	Experiment day power (used to indicate package is on or off)

Photons diffracted by the crystals are detected by the Geiger tubes. A fraction (depending on quantum efficiency) of these photons are absorbed by the Geiger counters and produce electric pulses; however, Appendix A gives corrections. The pulses from each tube are preamplified and sent to a counter-shift register. The counter-shift register counts the number of pulses received during the time between associated readout gates and transmits the number to the spacecraft memory during the readout gate.

There are two photon-counter data channels used by the instruments A and B. Counter-shift register A is read out on main-frame gate 2 and counter-shift register B is read out on main-frame gates 13 and 23.

Command 5 (S/C 127) latches a relay to connect the output of tube A and preamp A to counter-shift register A and similarly B to B. Command 6 (S/C 128) latches the relay to connect A to B and B to A.

Two 1200-volt power supplies furnish power to the Geiger tubes. Both tubes are energized by only one power supply at a time. Command 3 (S/C 125) latches a relay to apply power to high-voltage supply 1, while command 4 (S/C 126) latches the relay to supply power to supply 2.

The low-voltage power system is also redundant. Command 1 (S/C 123) latches a relay to apply power to low-voltage supply 1, while command 2 (S/C 124) latches the relay to apply power to low-voltage supply 2.

The NRL spectrometers and electronic equipment are shown in Fig. 1 and comprise half of the lefthand pointed section of the OSO-4 spacecraft, sharing a compartment with the American Science and Engineering (AS & E) instrument.

Data Format

The data format is given in Table 1. Shown are words peculiar to the NRL package and the housekeeping words of the spacecraft used for data reduction. The notation is the same as that used in the description of the telemetry.

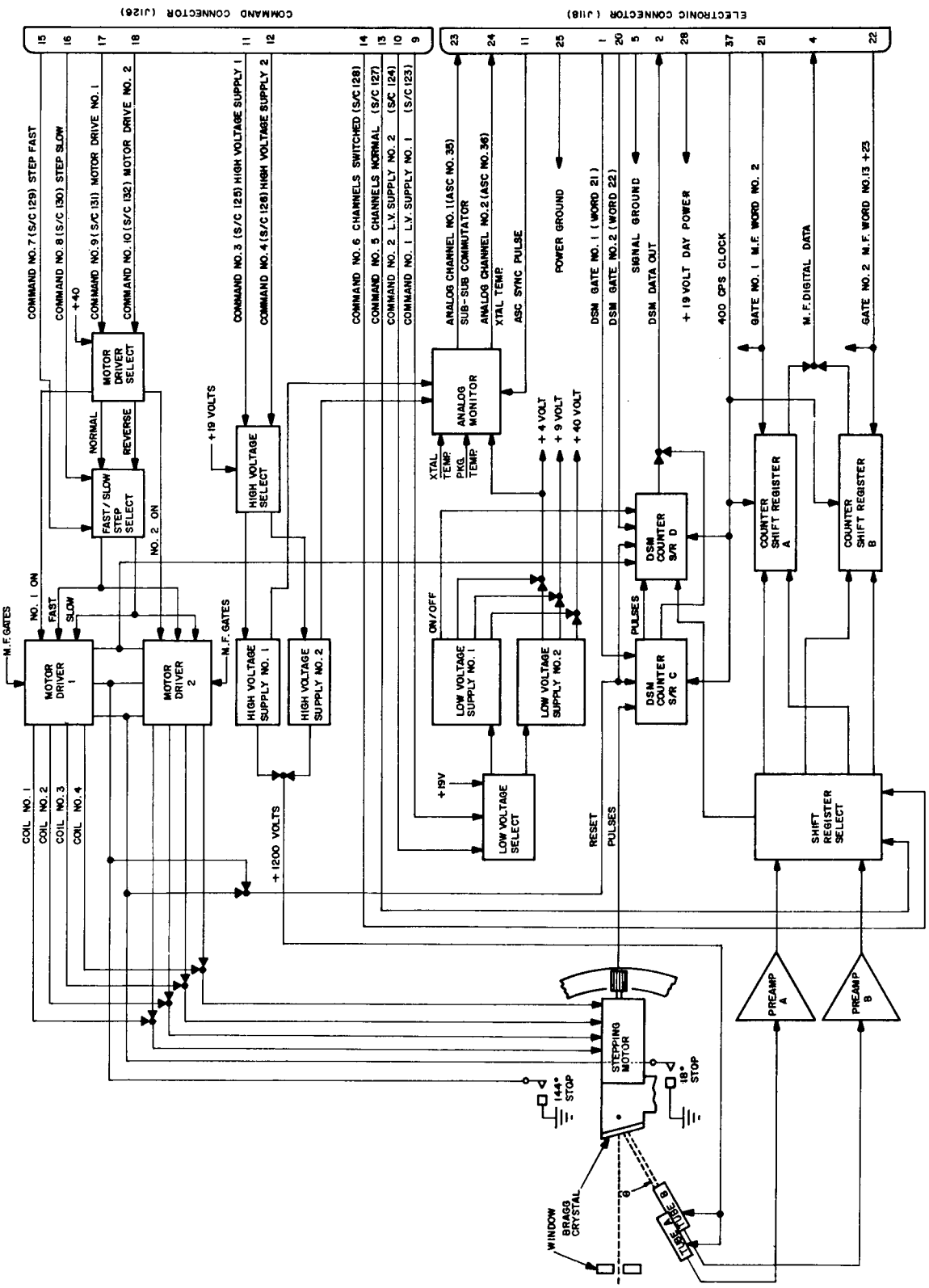

Fig. 6—Block diagram of the instrument electronics

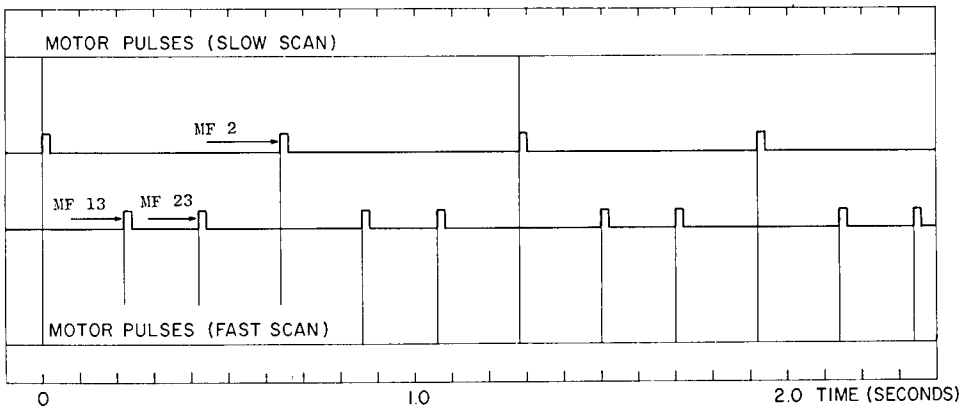

Fig. 7—The stepping motor timing with respect to word gates. The vertical lines indicate motor pulses for slow (upper lines) and fast (lower lines) stepping rates

DATA REDUCTION

The first step in the data reduction process is to display the count rate as a function of spectrometer step. The displays reveal dominant spectral features and allow data to be chosen for further reduction. It is also helpful to place a wavelength scale on the same plot. The wavelength is given by

$$n\lambda = 2d \sin \theta .$$

While there is some higher-order ($n \geqslant 2$) diffraction, nearly all the data are from first-order ($n = 1$) diffraction. The angle θ is the angle between the source direction and the atomic planes of the crystal and is given by

$$\theta = N\Delta + \varphi + \alpha ,$$

where

Δ = 0.1 degree

N = { Spectrometer steps (DSM - M = 0)
{ 660 - spectrometer steps (DSM - M = 1)

φ = { 9.778 degrees LiF
{ 8.984 degrees EDDT

α = { Elevation angle of the spacecraft above
{ the center of the solar disk

$2d$ = { 4.006 Å LiF
{ 8.798 Å EDDT

The parameters φ and 2d were derived from least-square fits to laboratory calibration data. This still does not completely specify the angle θ since the source (flare) may be anywhere on the solar disk and some misalignment occurred during the installation of

the NRL package. Further corrections may be made by using the Lyman-α lines of hydrogenic ions as reference wavelengths. Wavelengths of hydrogenic ions have been calculated with great precision by Garcia and Mack.* Any discrepancy found may then be applied uniformly to all θ values.

Examples of data from the two spectrometers are shown in Figs. 8, 9, and 10. Figures 8 and 9 compare scans from a typical active and a flaring sun; Fig. 10 is from scans with particle contamination.

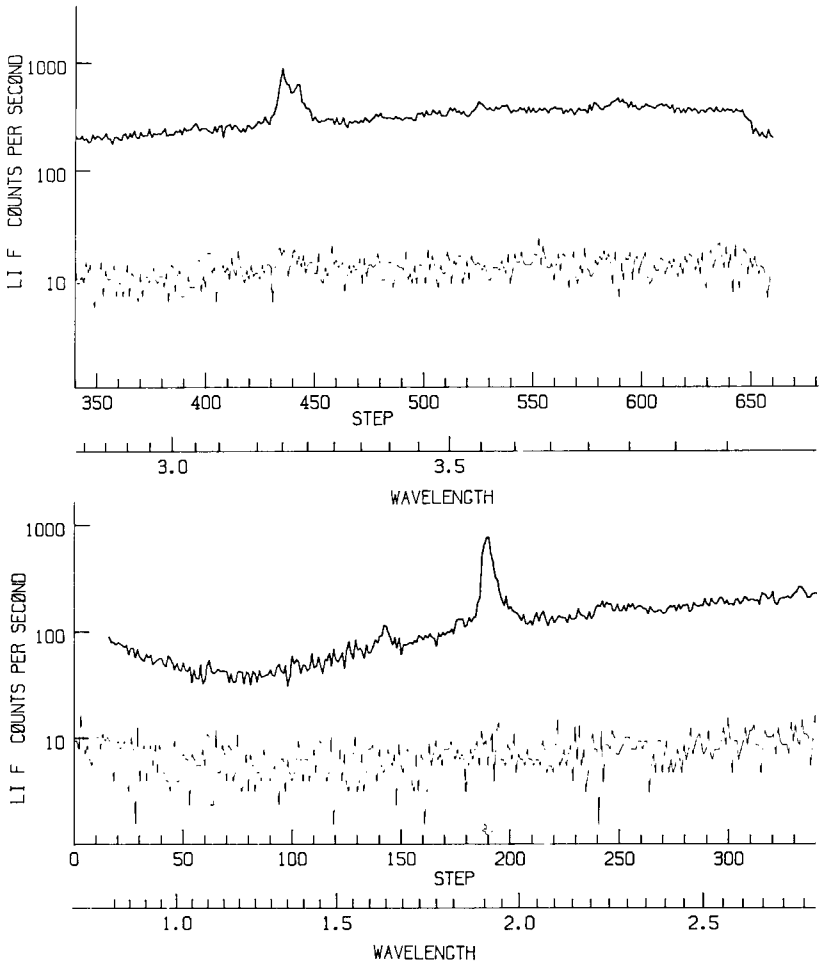

Fig. 8—Comparison of LiF spectrometer scans from a flaring (upper) and active (lower) sun

The next process required for data reduction is to find the rate of photon absorption by the detectors, which is given by (Appendix A)

$$R_p = \frac{R_c}{1 - \tau R_c} - R_B ,$$

where R_c is the observed count rate; R_B is the background count rate (determined from quiet spectral scans, no lines or particles, not a function of angle), approximately 8 counts/sec; and τ is the dead time of the Geiger counter, 200 μsec.

*J. D. Garcia and J. E. Mack, J. Opt. Soc. Am. 55, 654 (1965).

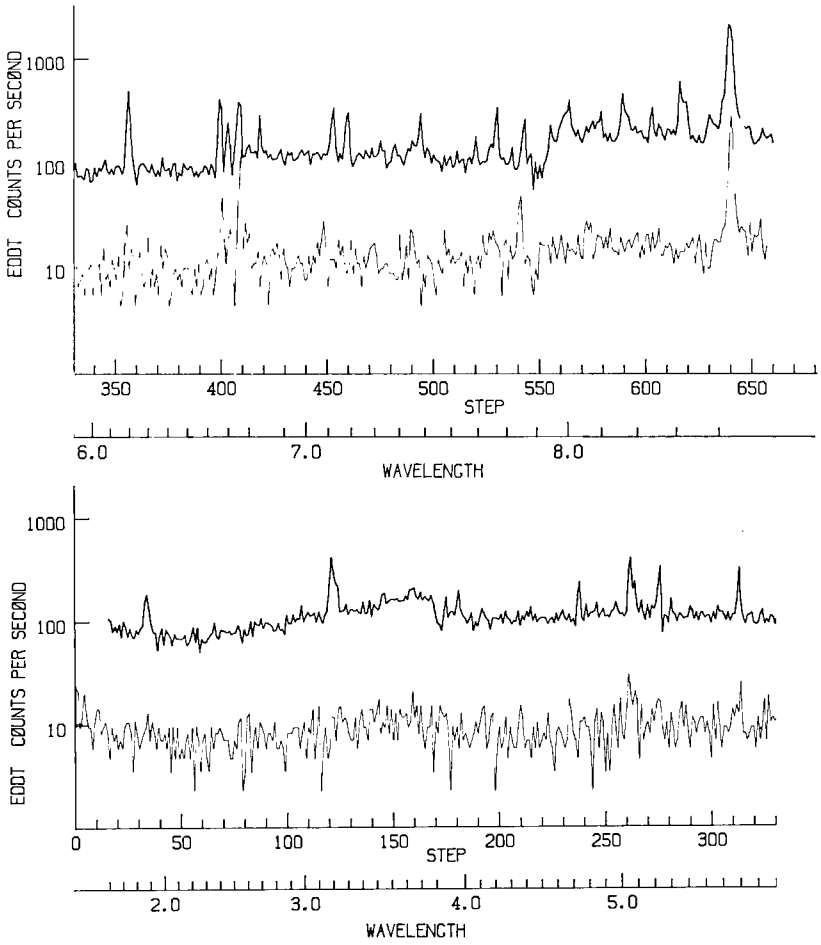

Fig. 9—Comparison of EDDT spectrometer scans from a flaring (upper) and active (lower) sun

The next step is to determine the photon flux incident on the instrument. From Fig. 3 it is obvious that the cross-sectional area depends on the angle; thus, this flux is given by

$$I_\theta = \frac{R_p}{\ell a \, RET} \quad \text{(photons/time-area-angle)},$$

where ℓ is the width of the detector windows, 0.419 cm; and

$$a = \text{lesser of} \begin{cases} q(\lambda/2d) \\ b \end{cases}$$

(q is the crystal length, 2.54 cm; b is the detector window length, 1.918 cm; and λ and 2d have been previously defined). The quantity RET is the combined effect of the reflectivity of the crystal, the quantum efficiency of the detector, and the transmission of the filter, and is given by

$$RET = \frac{Q}{\sqrt{(2d)^2 - \lambda^2}}$$

(Q is tabulated in Table 2 and shown in Figs. 11 and 12).

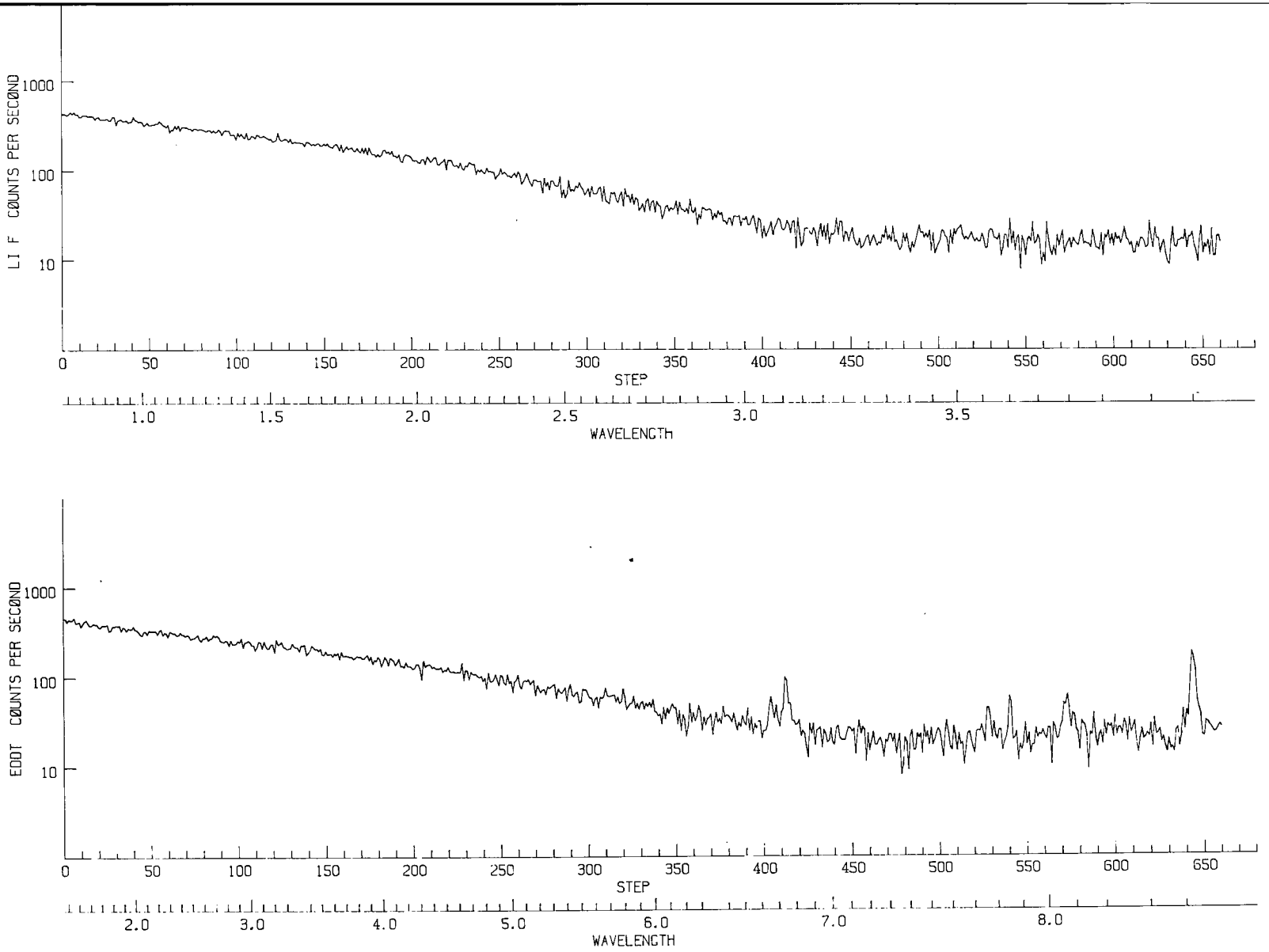

Fig. 10—Spectrometer scans with particle contamination

Table 2
Efficiency Parameters

λ(A)	Q(× 10^5)	λ(A)	Q(× 10^5)	λ(A)	Q(× 10^5)
EDDT					
1.5	2.817	3.8	1.291	6.1	0.373
1.6	2.160	3.85	1.204	6.2	0.359
1.7	1.878	3.88	0.939	6.3	0.347
1.8	1.667	3.9	0.789	6.4	0.336
1.9	1.502	3.95	0.775	6.5	0.324
2.0	1.408	4.0	0.763	6.6	0.322
2.05	1.371	4.1	0.749	6.65	0.331
2.1	1.338	4.2	0.735	6.7	0.376
2.2	1.298	4.3	0.716	6.75	0.432
2.3	1.275	4.4	0.700	6.8	0.451
2.4	1.258	4.5	0.683	6.85	0.460
2.5	1.249	4.6	0.664	6.9	0.455
2.6	1.246	4.7	0.643	7.86	0.282
2.7	1.246	4.8	0.622	7.9	0.432
2.8	1.249	4.9	0.599	7.95	0.643
2.9	1.256	5.0	0.575	7.98	0.674
3.0	1.263	5.1	0.554	8.0	0.676
3.1	1.277	5.2	0.531	8.1	0.678
3.2	1.291	5.3	0.512	8.2	0.678
3.3	1.305	5.4	0.493	8.3	0.683
3.4	1.322	5.5	0.472	8.4	0.695
3.5	1.336	5.6	0.451	8.5	0.709
3.6	1.347	5.7	0.434	8.6	0.728
3.65	1.350	5.8	0.420	8.7	0.754
3.7	1.343	5.9	0.404	8.76	0.770
3.75	1.326	6.0	0.387	—	—
LiF					
1.5	1.750	2.45	3.205	3.4	2.580
1.55	2.150	2.5	3.150	3.42	2.580
1.6	2.500	2.55	3.100	3.44	2.725
1.65	2.780	2.6	3.040	3.45	2.835
1.7	2.980	2.65	2.985	3.5	2.85
1.75	3.150	2.7	2.930	3.55	2.845
1.8	3.290	2.75	2.880	3.6	2.835
1.85	3.400	2.8	2.825	3.65	2.820
1.9	3.485	2.85	2.79	3.7	2.810
1.95	3.535	2.9	2.755	3.75	2.800
2.0	3.550	2.95	2.735	3.8	2.790
2.05	3.550	3.0	2.715	3.85	2.770
2.10	3.530	3.05	2.700	3.87	2.700
2.15	3.500	3.1	2.680	3.88	1.800
2.2	3.450	3.15	2.660	3.89	1.515
2.25	3.405	3.2	2.650	3.91	1.495
2.3	3.355	3.25	2.630	3.94	1.480
2.35	3.305	3.3	2.610	3.97	1.485
2.4	3.255	3.35	2.590	3.99	1.490

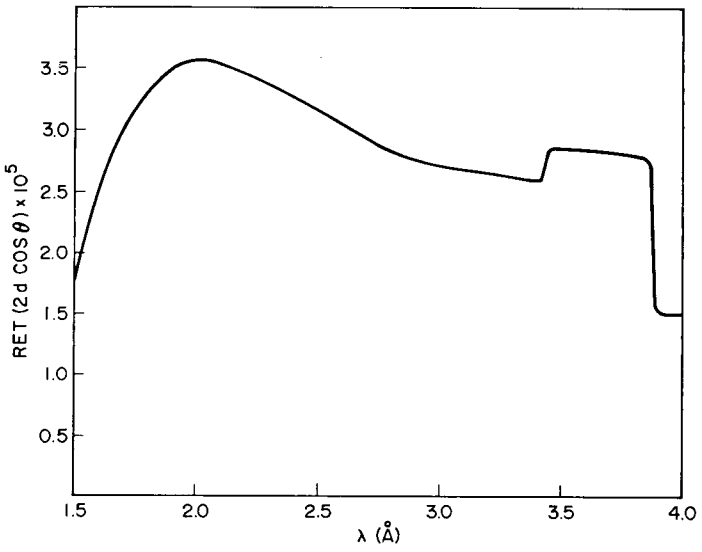

Fig. 11—Plot of Q (= RET X 2d cos θ) vs wavelength for the LiF spectrometer

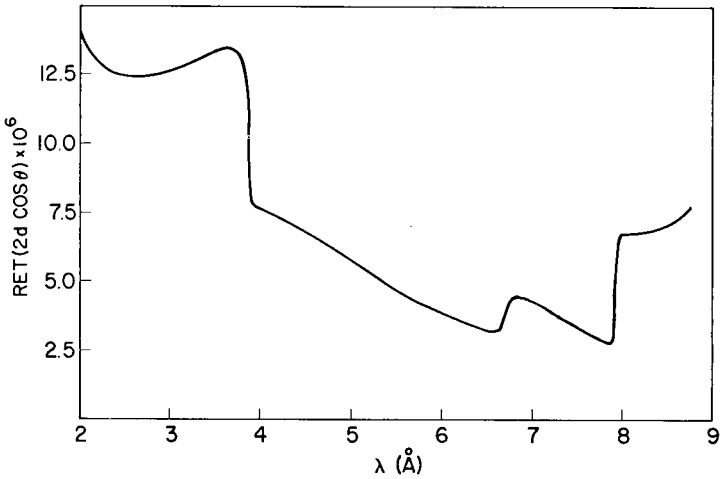

Fig. 12—Plot of Q (= RET X 2d cos θ) vs wavelength for the EDDT spectrometer

At this point, I_θ is displayed as a function of the angle, and it is possible to separate the line and continuum fluxes $I_\theta{}^L + I_\theta{}^c$. This is accomplished by smoothing $I_\theta{}^c$(avoiding lines and edges) and interpolating under the lines. The total photon flux in a line is then (Appendix B)

$$I^L = \sum I_\theta{}^L \Delta\theta ,$$

where $\Delta\theta$ = 0.001745 radian. The final step in the process is to find I_λ by (Appendix B)

$$I_\lambda = \frac{I_\theta{}^c}{\sqrt{(2d)^2 - \lambda^2}} + \sum I^L S(\lambda, \lambda_0) ,$$

where the sum is over all lines.

The function $S(\lambda, \lambda_0)$ is the profile of a line centered at λ_0 and for thin plasmas is usually taken to be a Gaussian of the form

$$S(\lambda, \lambda_0) = \left(\frac{mc^2}{2\pi kT\lambda_0{}^2}\right)^{1/2} e^{-\frac{mc^2}{2kT\lambda_0{}^2}(\lambda-\lambda_0)^2},$$

where m is the mass of the ion forming the line, c is the velocity of light, k is Boltzmann's constant, and T is the kinetic temperature of the ions.

APPENDIX A
DEAD TIME CORRECTION

For many photon-counting detectors and for nearly all pulse-counting circuitry there is a time τ following a detected pulse when no more pulses may be detected. This time ranges from a fraction of a microsecond to seconds depending on the given counters and circuitry.

If we assume Poisson statistics (i.e., the time of arrival of a photon is independent of the times of arrival of any previous photons), the probability that n photons will be absorbed in a time interval τ is

$$P_n = e^{-R_p\tau} \frac{(R_p\tau)^n}{n!},$$

where R_p is the rate at which photons are being absorbed. Thus, the mean number of photons absorbed in a time τ is

$$N_\tau = \sum_{n=0}^{\infty} nP_n = R_p\tau .$$

Suppose that n_c is the number of photons detected (not absorbed) in a time period T. Then the number of photons absorbed in this time is R_pT. Thus, since $R_p\tau$ are absorbed but not counted for every count n_c

$$n_c = R_pT - R_p\tau n_c ;$$

then

$$R_p = \frac{n_c/T}{1 - \tau(n_c/T)} .$$

But n_c/T is the observed count rate.

This correction is used to determine the rate at which photons are absorbed and becomes important ($\gtrsim 10\%$) when the product of the dead time τ and count rate n_c/T exceeds 0.1.

APPENDIX B
CRYSTAL EFFECTS OF BENDING

Suppose we have a source which gives a single monochromatic line. The diffracted radiation from a flat crystal will show a peak at an angle

$$\theta' = \sin^{-1}\left(\frac{\lambda}{2d}\right) \tag{A1}$$

and a spread which we take to be approximately Gaussian in shape. We may then define a reflectivity as

$$R_\theta = \frac{R_0}{f\sqrt{k\pi}} e^{-(\theta-\theta')/f^2k} \tag{A2}$$

where $2f$ is the FWHM of the reflectivity curve, R_0 is the integrated reflectivity

$$R_0 = \int_{-\infty}^{\infty} R_\theta \, d\theta$$

and

$$e^{-(1/k)} = \frac{1}{2}$$

(i.e., $k = 1.44269$).

Let us assume that even if we had an ideal crystal (i.e., $R_0 = 1$, and $f = 0$), the diffracted radiation due to the line profile would still be of the form

$$I_\theta = \frac{I_0}{g\sqrt{k\pi}} e^{-(\theta-\theta_0{}^2)/g^2k}, \tag{A3}$$

where $2g$ is the FWHM and the total intensity of the line is

$$I_0 = \int_{-\infty}^{\infty} I_\theta \, d\theta.$$

For a slightly bent crystal, we would expect that each segment i would have the property

$$R_{\theta i} = \frac{R_{0i}}{f\sqrt{k\pi}} e^{-(\theta_i - \theta')^2/f^2k},$$

where $\theta_i = \theta'$ is the angle at which the peak reflectivity would occur for the ith segment in accordance with Eq. (A1). We set $\theta_i = h(s_i)$, where s_i is the distance along the crystal of the ith segment. Further,

$$R_{\theta i} = R_0 r(s_i) \frac{(\Delta s)_i}{\ell},$$

where ℓ is the length of the crystal, $(\Delta s)_i$ is the width of the ith segment, and $r(s_i)$ is a function describing any inhomogeneities of the integrated reflectivity of each crystal segment and is normalized such that

$$\int_{-\ell/2}^{\ell/2} r(s_i)\, ds = \ell.$$

Then

$$R_\theta = \frac{R_0}{f\ell\sqrt{k\pi}} \int_{-\ell/2}^{\ell/2} r(s) e^{-[h(s)-\theta']^2/f^2k}\, ds. \tag{A4}$$

For a plane crystal, h(s) = const = θ, and we have again, the previous description given in Eq. (A2).

Let us now include the spread of the line given in Eq. (A3) with the spread of the crystal expressed in Eq. (A4). Then

$$I_\theta = \frac{I_0 R_0}{g\ell fk\pi} \int_{-\infty}^{\infty} e^{-(\theta'-\theta_0)^2/g^2k}\, d\theta' \int_{-\ell/2}^{\ell/2} r(s) e^{-[h(s)-\theta']^2/f^2k}\, ds.$$

Now let us reference the angle h(s) to the angle the center of the crystal makes with the incident radiation (i.e., h(s) becomes $\psi(s) + \theta_c$ and $\psi(0) = 0$). Then

$$I_{\theta_c} = \frac{I_0 R_0}{\ell fgk\pi} \int_{-\ell/2}^{\ell/2} r(s)\, ds \int_{-\infty}^{\infty} \exp\left\{-(\theta' - \theta)^2/g^2k - [\psi(s) + \theta_c - \theta']^2/f^2k\right\} d\theta'.$$

This expression reduces to

$$I_{\theta_c} = \frac{I_0 R_0}{\ell\sqrt{k\pi(f^2 + g^2)}} \int_{-\ell/2}^{\ell/2} r(s) \exp\left\{-[\theta_c + \psi(s) - \theta_0]^2/k(f^2 + g^2)\right\} ds. \tag{A5}$$

Now, suppose we sum over the stepped angles θ_c and let r(s) = 1:

$$\sum_{n=-\infty}^{\infty} I_{\theta_c}\Delta\theta = \frac{I_0R_0}{\ell\sqrt{k\pi(g^2+f^2)}}\sum_{n=-\infty}^{\infty}\Delta\theta\int_{-\ell/2}^{\ell/2}\exp\left\{-[n\Delta\theta+\psi(s)-\theta_0]^2/k(f^2+g^2)\right\}ds, \tag{A6}$$

where we have set $\theta_c = n\Delta\theta$.

For a plane crystal $\psi(s) = 0$, Eq. (A6) becomes

$$\sum_{n=-\infty}^{\infty} I_{\theta_c}\Delta\theta = \frac{I_0R_0}{\sqrt{k\pi(f^2+g^2)}}\sum_{n=-\infty}^{\infty}\exp\left[-(n\Delta\theta-\theta_0)^2/k(f^2+g^2)\right].$$

For values of $\Delta\theta/\sqrt{k(f^2+g^2)} \lesssim 1$, this becomes

$$\sum_{n=-\infty}^{\infty} I_{\theta_c}\Delta\theta = I_0R_0. \tag{A7}$$

Now for a uniformly bent, homogeneous crystal, r(s) = 1 and $\psi(s) = \xi s$. If the angle of bend is just the width of a step, then $\Delta\theta = \xi\ell$. Thus, Eq. (A6) becomes

$$\sum_{n=-\infty}^{\infty} I_{\theta_c}\Delta\theta = \frac{I_0R_0}{\sqrt{k\pi(f^2+g^2)}}\sum_{n=-\infty}^{\infty}\int_{-\ell/2}^{\ell/2}\xi\exp\left\{-[n\xi\ell+\xi s-\theta_0]^2/k(f^2+g^2)\right\}ds.$$

But the sum and integral may be replaced by a single integral, so we have

$$\sum_{n=-\infty}^{\infty} I_{\theta_c}\Delta\theta = \frac{I_0R_0}{\sqrt{k\pi(f^2+g^2)}}\int_{-\infty}^{\infty}\xi\exp\left\{-[\xi s-\theta_0]^2/k(f^2+g^2)\right\}ds.$$

$$= I_0R_0,$$

which is the same as Eq. (A7).

For continuum (approximately flat)

$$I_\lambda \approx \frac{1}{\Delta\lambda}\int_{\Delta\lambda} I_\lambda\, d\lambda$$

$$\approx \frac{1}{\Delta\lambda}\int_{\Delta\lambda} I_\theta\, d\theta$$

$$\approx I_\theta\left(\frac{\Delta\theta}{\Delta\lambda}\right) = I_\theta/\sqrt{(2d)^2-\lambda^2}$$

which is derived from Eq. (A1).

Security Classification

DOCUMENT CONTROL DATA - R & D

(Security classification of title, body of abstract and indexing annotation must be entered when the overall report is classified)

1. ORIGINATING ACTIVITY *(Corporate author)* Naval Research Laboratory Washington, D.C. 20390	2a. REPORT SECURITY CLASSIFICATION UNCLASSIFIED 2b. GROUP

3. REPORT TITLE

THE NRL OSO-4 BRAGG CRYSTAL SPECTROMETER INSTRUMENT

4. DESCRIPTIVE NOTES *(Type of report and inclusive dates)*
An interim report on a continuing NRL problem

5. AUTHOR(S) *(First name, middle initial, last name)*
J.F. Meekins

6. REPORT DATE	7a. TOTAL NO. OF PAGES	7b. NO. OF REFS
July 27, 1972	24	1

8a. CONTRACT OR GRANT NO.	9a. ORIGINATOR'S REPORT NUMBER(S)
NRL Problem A01-29 b. PROJECT NO.	NRL Report 7423
c. d. S-99805-G	9b. OTHER REPORT NO(S) *(Any other numbers that may be assigned this report)*

10. DISTRIBUTION STATEMENT
Approved for public release; distribution unlimited

11. SUPPLEMENTARY NOTES	12. SPONSORING MILITARY ACTIVITY
National Aeronautics and Space Admin. Goddard Space Flight Center Greenbelt, Maryland 20771	

13. ABSTRACT

Two Bragg crystal spectrometers were placed on the OSO-4 satellite to study solar flare plasmas by their spectral emissions. The solar flare plasma parameters were measured with these spectrometers, which together covered a total wavelength range of 0.6 to 8.4 Å. With these instruments, knowledge could be gained into the mechanisms governing the plasma behavior in the high temperature-low density regime of flare production and in solar evolution and elemental abundances in the sun. However, spacecraft limitations forced many restrictions on the design of the instrument, so the final instrument could not measure all the solar flare plasma state parameters.

DD FORM 1 NOV 65 1473
S/N 0101-807-6801

Security Classification

14. KEY WORDS	LINK A		LINK B		LINK C	
	ROLE	WT	ROLE	WT	ROLE	WT
OSO-4 pointed instrument Solar flares X-ray spectroscopy						